Bull Earthquake Eng (2014) 12:2507–2530
DOI 10.1007/s10518-014-9603-3

ORIGINAL RESEARCH PAPER

Loading protocols for European regions of low to moderate seismicity

Panagiotis E. Mergos · Katrin Beyer

Received: 19 July 2013 / Accepted: 16 February 2014 / Published online: 9 March 2014

Abstract Existing loading protocols for quasi-static cyclic testing of structures are based on recordings from regions of high seismicity. For regions of low to moderate seismicity they overestimate imposed cumulative damage demands. Since structural capacities are a function of demand, existing loading protocols applied to specimens representative of structures in low to moderate seismicity regions might underestimate structural strength and deformation capacity. To overcome this problem, this paper deals with the development of cyclic loading protocols for European regions of low to moderate seismicity. Cumulative damage demands imposed by a set of 60 ground motion records are evaluated for a wide variety of SDOF systems that reflect the fundamental properties of a large portion of the existing building stock. The ground motions are representative of the seismic hazard level corresponding to a 2 % probability of exceedance in 50 years in a European moderate seismicity region. To meet the calculated cumulative damage demands, loading protocols for different structural types and vibration periods are developed. For comparison, cumulative seismic demands are also calculated for existing protocols and a set of records that was used in a previous study on loading protocols for regions of high seismicity. The median cumulative demands for regions of low to moderate seismicity are significantly less than those of existing protocols and records of high seismicity regions. For regions of low to moderate seismicity the new protocols might therefore result in larger strength and deformation capacities and hence in more cost-effective structural configurations or less expensive retrofit measures.

P. E. Mergos · K. Beyer (✉)
École Polytechnique Fédérale de Lausanne (EPFL), Lausanne, Switzerland
e-mail: katrin.beyer@epfl.ch

Present address
P. E. Mergos
City University London, Northampton Square, London EC1V 0HB, UK
e-mail: panagiotis.mergos.1@city.ac.uk

K. Beyer
EPFL ENAC IIC EESD, GC B2 504 (Bâtiment GC), Station 18, Office GCB2504,
1015 Lausanne, Switzerland

Keywords Quasi-static · Loading protocol · Seismic demands · Cumulative damage · Low to moderate seismicity

1 Introduction

Performance-based earthquake design and assessment requires reliable estimates of structural members' strength and deformation capacities. These capacities can often not be predicted accurately by analytical or numerical modelling and experimental testing is required. Most commonly, quasi-static cyclic tests are conducted where predefined displacement histories, named loading protocols, are applied at slow rates. When subjected to cyclic loading, strength and in particular deformation capacity of structural components depend on the imposed cumulative damage demand (Krawinkler et al. 2001). Hence, in order to yield realistic capacity estimates, loading protocols must reflect the estimated cumulative seismic demands for the region of interest. Gatto and Uang (2003), for example, examined the effects of the imposed loading protocols on the structural capacities of woodframe shear walls. They observed that woodframe shear walls subjected to the SPD loading protocol (Porter 1987), which is known to overestimate seismic demands even for regions of high seismicity, had in average a 25 % lower ultimate strength capacity and a 47 % lower ultimate deformation capacity than woodframe shear walls tested with the CUREE protocol for ordinary ground motions (Krawinkler et al. 2001), which represents better the anticipated seismic demand for regions of high seismicity. Moreover, the failure type observed for the SPD protocol was not the one developed in real earthquakes.

Several loading protocols have been developed in the literature for different types of structural and non-structural components. A list of these protocols includes but is not limited to: SPD protocol (Porter 1987), ATC-24 protocol (ATC 1992), Crescendo protocol (Behr and Belarbi 1996), SAC protocol (Clark et al. 1997), protocol for steel moment frames (Krawinkler et al. 2000), CUREE protocols (Krawinkler et al. 2001), EN-12512 protocol (EN 2001), AISC protocol (AISC 2005), protocol for short links in eccentrically braced frames (Richards and Uang 2006), FEMA-461 protocols (FEMA-461 2007), ISO protocol (ISO 2010), SUNY-Buffalo NCS protocol (Retamales et al. 2011) and the protocol for non-structural window systems (Hutchinson et al. 2011).

All of the above protocols have been developed for regions of high seismicity. However, earthquakes in these regions impose in average higher cumulative damage demands than earthquakes in regions of low to moderate seismicity (Kramer 1996). Hence, existing loading protocols may overestimate seismic demands for regions of low to moderate seismicity and therefore underestimate force and/or deformation capacity leading to uneconomic or even unfeasible structural designs and retrofit solutions.

Furthermore, many of the existing loading protocols have not been developed to conform to the performance objectives prescribed in modern seismic design codes like EC8-Part 3 (CEN 2005). More specifically, they have been developed for seismic hazard levels corresponding to the 10 % probability of exceedance in 50 years and not the 2 % probability of exceedance in 50 years, which is the basis for determining displacement capacities in accordance with EC8-Part 3 as will be explained in Sect. 2.1.

This study develops quasi-static cyclic loading protocols representative of the seismic demand in European low to moderate seismicity regions. The protocols are applicable to a wide range of structures and were derived by developing a methodology of four steps: (1) selection and scaling of ground motion records; (2) selection of representative structural

systems; (3) calculation of cumulative seismic demands and (4) construction of loading protocols. The following sections outline these steps in detail.

2 Selection and scaling of ground motions

2.1 Seismic hazard level

EC8-Part 3 deals with the assessment and retrofitting of buildings (CEN 2005) and has fully adopted the performance-based approach (Fardis 2009). It addresses three distinguished limit states: "Damage Limitation" (DL), "Significant Damage" (SD) and "Near Collapse" (NC) limit state. According to EC8-Part 3, the protection normally considered appropriate for ordinary new buildings is achieved by selecting the following values for the return periods: a 225 years return period (20 % probability of exceedance in 50 years) for the DL limit state, a 475 years return period (10/50) for the SD limit state and a 2,475 years return period (2/50) for the NC limit state. The design objectives in EC8-Part 3 for non-brittle structural failures are satisfied when the deformation demands for each seismic hazard level do not exceed the respective deformation capacities for the corresponding performance level.

EC8-Part 3 defines deformation capacities Δ_{NC} at the NC performance level as the deformation related to a 20 % drop of the peak strength. Deformation capacities Δ_{SD} for the SD performance level are then determined as a fraction of Δ_{NC} (e.g. 75 % for concrete members and unreinforced masonry piers). Hence, in order to calculate deformation capacities for both limit states, Δ_{NC} needs to be estimated.

Unlike often assumed, force and deformation capacities of structural members are not independent of, but are rather related to demands. Hence, in order to establish by means of quasi-static cyclic testing reliable estimates of Δ_{NC} that are consistent with EC8 design objectives, the imposed loading protocol should represent the 2/50 seismic hazard level. For this reason, selection and scaling of the ground motion records in this study aim at representing the cumulative demand imposed by this seismic hazard level.

2.2 Selection of ground motion records

This section presents the selection and scaling of ground motion records representative of European regions of low to moderate seismicity for the 2/50 seismic hazard level. The city of Sion in Switzerland is used as a representative region of low to moderate seismicity. It is situated in the Rhone Valley and the design peak ground acceleration (PGA) for ground type C is $0.16 \cdot 1.15 = 0.184$ g for the 10/50 hazard level. For this site, de-aggregation of hazard results for the 2/50 seismic hazard level are readily available (Giardini et al. 2004).

The criteria applied for selecting the ground motion records are the following:

- Only real records are used since artificial records do not always reflect the real phasing of seismic waves, cycles of motion and therefore input energy (Iervolino et al. 2008).
- Ordinary and not near fault records (characterized by long-period velocity pulses) are selected. This decision assures more conservative estimates of the number of cycles and the imposed cumulative damage effects (CDEs) (Krawinkler et al. 2001).
- All records stem from the European Strong Motion Database (Ambraseys et al. 2004).
- Magnitude-distance pairs (M, R) of the selected records are compatible with the de-aggregation results from the probabilistic hazard analysis for the site of Sion and the 2/50 seismic hazard level. All ground motions have therefore a moment magnitude within the range $4.3 \leq M_w \leq 6.6$ and an epicentral distance within the range $5 \leq R \leq 33$ km. Not

only the overall magnitude and distance ranges, but also the distribution of the selected ground motion (M, R) pairs reflect Sion's de-aggregation results.
- Accelerograms recorded only at ground types B and C according to EC8-Part 1 classification are selected, which represent the most common types of soil. Similar soil types in terms of average shear wave velocity have been considered by Krawinkler et al. (2001). This means that rock sites (ground type A) and very soft soil sites (ground types D and E) are not examined herein.
- Typically only one record per seismic event is selected. This is done in order to avoid a bias towards a particular seismic event. However, in limited cases where seismic events were recorded at significantly different epicentral distances more than one record is selected.
- All ground motion records have PGAs higher than 0.04 g. This criterion is used in order to avoid large scaling factors. Furthermore, it is consistent with the very low seismicity limit recommended by EC8-Part 1 below which seismic provisions do not need to be applied (EC8-Part 1 §3.2.1(5)).

By applying the afore-described criteria, 60 ground motion records were selected. The characteristics of these records are summarized in Table 1. In addition to the 60 ground motion records representative of low to moderate seismicity regions, the 20 ground motion records employed for developing several protocols for high seismicity regions (e.g. Krawinkler et al. 2001; FEMA-461 2007) are also examined for comparison reasons.

The loading protocols developed in this study aim at representing cumulative seismic demands of a main shock. Foreshocks, aftershocks or even the complete earthquake sequence a structure may face during its lifetime could also be considered for the derivation of loading protocols but this is outside the scope of this study.

2.3 Scaling of ground motion records

The selected ground motion records are scaled one by one in order to match the spectral acceleration of the horizontal elastic spectrum of EC8 for the 2/50 seismic hazard level at the fundamental period of the structure. The same procedure was adopted by Krawinkler et al. (2001). The target EC8 elastic spectrum is derived for soil class C. The PGA for the 2/50 seismic hazard level is calculated by multiplying the PGA for the 10/50 hazard level by the importance factor γ_I in EC8-Part 1 (Eurocode 2004):

$$\gamma_I = \left(\frac{P_L}{P_{LR}}\right)^{-1/k} = \left(\frac{2}{10}\right)^{-1/3} \approx 1.71 \tag{1}$$

In this equation, P_L is the target probability of exceedance in 50 years (2 %) and P_{LR} is the reference probability of exceedance in 50 years (10 %). The parameter k is an exponent that depends on the seismicity and which, according to EC8, is generally of the order of 3. The PGA on rock for the 10/50 seismic hazard level and the site of Sion is taken equal to 0.16 g (SIA 2003), while for the high seismicity earthquakes it is taken equal to 0.40 g. The latter value applied to the EC8 spectrum yields the same plateau acceleration as the response spectrum employed in the study by Krawinkler et al. (2001) who examined the seismic demand for regions of high seismicity for the 10/50 hazard level.

Table 1 Ground motion records representative for European low to moderate seismicity regions

Earthquake name	Year	Distance R (km)	Magnitude M_w	PGA (g)	Ground type	Direction
Sarti	1993	8	4.3	0.06	B	Y
Kyllini (aftershock)	1988	10	4.3	0.04	B	X
Near E coast of Zakynthos	1990	5	4.5	0.04	B	Y
Pyrgos (aftershock)	1993	10	4.8	0.05	C	Y
Almiros (aftershock)	1980	10	4.8	0.06	B	X
Friuli (aftershock)	1976	10	4.9	0.08	B	Y
Patras	1988	5	4.9	0.11	B	X
Pyrgos (foreshock)	1993	7	4.9	0.10	C	X
Levkas island	1994	9	4.9	0.06	B	X
Izmit (aftershock)	1999	9	4.9	0.11	C	X
Ierissos	1983	8	5.1	0.13	B	X
Paliouri	1994	5	5.1	0.06	B	X
Campano Lucano (aftershock)	1981	5	5.2	0.07	B	X
Near coast of Preveza	1985	13	5.2	0.05	B	X
Kozani (aftershock)	1995	9	5.2	0.16	B	Y
Friuli (aftershock)	1976	15	5.3	0.11	B	Y
Dursunbey	1979	6	5.3	0.29	B	Y
Gulf of Corinth	1993	10	5.3	0.07	B	X
Umbria Marche (aftershock)	1997	7	5.3	0.13	C	Y
Etolia	1988	20	5.3	0.04	B	Y
Javakheti Highland	1990	15	5.4	0.04	B	Y
Pyrgos	1993	10	5.4	0.15	C	X
Komilion	1994	12	5.4	0.06	B	Y
Umbria	1984	19	5.6	0.21	B	X
Racha (aftershock)	1991	17	5.6	0.08	B	X
Umbria Marche (aftershock)	1997	20	5.6	0.10	B	X
Umbria Marche (aftershock)	1997	13	5.6	0.09	C	X
Patras	1993	10	5.6	0.19	B	Y
Kefallinia island	1992	14	5.6	0.23	B	Y
Masjed-E-Soleyman	2002	13	5.6	0.06	B	Y
Umbria Marche	1997	25	5.7	0.07	C	Y
Harbiye	1997	19	5.7	0.13	B	X
Ionian	1973	15	5.8	0.25	C	Y
Valnerina	1979	23	5.8	0.04	B	X
Lazio Abruzzo	1984	16	5.9	0.15	C	X
Kalamata	1986	10	5.9	0.30	B	Y
Kyllini	1988	14	5.9	0.15	B	X
Chenoua	1989	29	5.9	0.29	C	X
Firuzabad	1994	20	5.9	0.04	B	X
Firuzabad	1994	7	5.9	1.06	B	Y
Friuli (aftershock)	1976	9	6	0.11	C	X

Table 1 continued

Earthquake name	Year	Distance R (km)	Magnitude M_w	PGA (g)	Ground type	Direction
Basso Tirreno	1978	18	6	0.07	C	X
Umbria Marche	1997	11	6	0.52	B	X
Umbria Marche	1997	23	6	0.08	B	Y
Ano Liosia	1999	20	6	0.16	B	Y
Ano Liosia	1999	14	6	0.31	B	Y
Mt. Vatnafjoll	1987	31	6	0.06	B	Y
Faial	1998	11	6.1	0.42	C	X
Volvi	1978	29	6.2	0.15	C	Y
Montenegro (aftershock)	1979	8	6.2	0.27	B	Y
Montenegro (aftershock)	1979	21	6.2	0.17	B	X
Kefallinia (aftershock)	1983	9	6.2	0.23	B	Y
Alkion	1981	25	6.3	0.12	C	Y
Adana	1998	30	6.3	0.27	C	Y
Dinar	1995	8	6.4	0.32	C	Y
South Iceland (aftershock)	2000	12	6.4	0.39	B	Y
South Iceland (aftershock)	2000	21	6.4	0.16	B	Y
South Iceland	2000	17	6.5	0.40	B	X
Alkion	1981	19	6.6	0.17	C	Y
Panisler	1983	33	6.6	0.13	B	X

3 Selection of representative structural systems

Cumulative damage effects imposed by ground motions are strongly dependent on the type of structural system. Hence, structural systems representative of those that will be tested need to be examined when developing loading protocols. In this study, the following structural systems are considered: elastic systems, systems for which lateral resistance is provided by timber walls, reinforced concrete (RC) frames, RC walls, unreinforced masonry shear or rocking walls.

SDOF systems are employed to model the structural response. Previous studies comparing SDOF and MDOF systems (FEMA-461 2007) have revealed that for short-period MDOF systems the demand on the structural components is well correlated with the demand on the SDOF system representing the first mode. For long-period MDOF systems, higher mode effects may become more important. However, as it will be shown in the following, CDEs for long-period systems are much less significant than for short-period systems. Hence, only SDOF systems are considered within the scope of this study. Nevertheless, it should be kept in mind that the proposed loading protocols are not representative of structural systems with important higher mode effects or MDOF systems with a strong concentration of inelastic deformations (e.g. soft storeys).

To be representative of a particular structural system, the SDOF system has to be assigned an appropriate force-displacement hysteretic model (Fig. 1). Table 2 summarizes the structural systems and the corresponding hysteretic models employed in this study. Following the suggestions by Priestley et al. (2007), the 'fat' Takeda hysteretic model is applied for

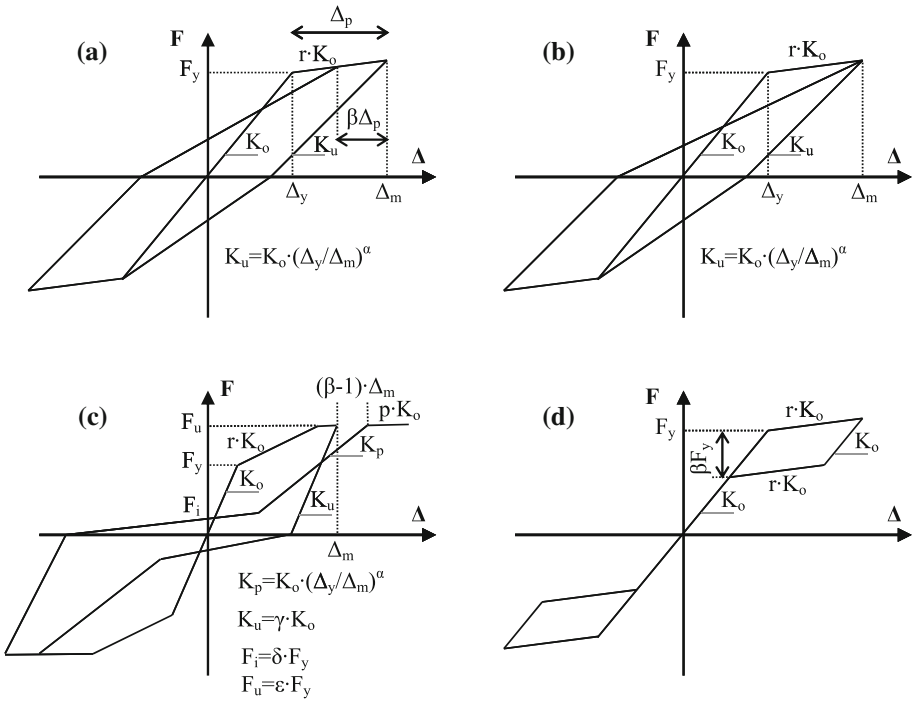

Fig. 1 Implemented hysteretic models: **a** 'Fat' Takeda ($\alpha = 0.3, \beta = 0.6$); **b** 'Thin' Takeda ($\alpha = 0.5$); **c** Wayne Stewart ($\alpha = 0.38, \beta = 1.09, \gamma = 1.45, \delta = 0.25, \varepsilon = 1.5, p = 0$); **d** *flag-shaped* ($\beta = 0.10$)

Table 2 Characteristics of SDOF systems representing different structural systems

Structural system	Hysteretic model	T (s)	r	q-factor
Infinitely elastic	Elastic (EL)	0.10, 0.20, 0.30, 0.50, 0.75, 1.00, 1.50	–	–
Timber walls	Wayne Stewart (WS)	0.10, 0.20, 0.30, 0.50, 0.75, 1.00, 1.50	0.001, 0.01, 0.10, 0.40	1.0, 2.0, 3.0, 4.0, 5.0
RC frames	'Fat' Takeda (FT)	0.15, 0.30, 0.50, 0.75, 1.00, 1.25, 1.50	0.001, 0.01, 0.05, 0.10	1.0, 2.0, 3.0, 4.5, 6.0
RC and masonry shear walls	'Thin' Takeda (TT)	0.10, 0.20, 0.30, 0.50, 0.75, 1.00, 1.50[a]	0.001, 0.01, 0.05, 0.10	1.0, 2.0, 3.0, 4.5, 6.0[a]
Masonry rocking walls	Flag shaped (FS)	0.10, 0.20, 0.30, 0.50, 0.75, 1.00, 1.50	0.001, 0.005, 0.01, 0.05	1.0, 1.5, 2.0, 2.5, 3.0

[a] For masonry shear walls only q-factor values of 1, 2 and 3 and vibration periods up to 0.5 s are examined

RC frames and the 'thin' Takeda hysteretic model for RC walls. The latter can also be used as rough approximation of the hysteretic response of unreinforced masonry shear walls (Aldemir et al. 2013; Ali et al. 2014). For rocking masonry walls a flag-shaped hysteretic model is chosen. The Wayne Stewart hysteretic model is adopted for timber walls with the hysteretic parameter values that Stewart (1987) proposed for plywood sheathed timber walls.

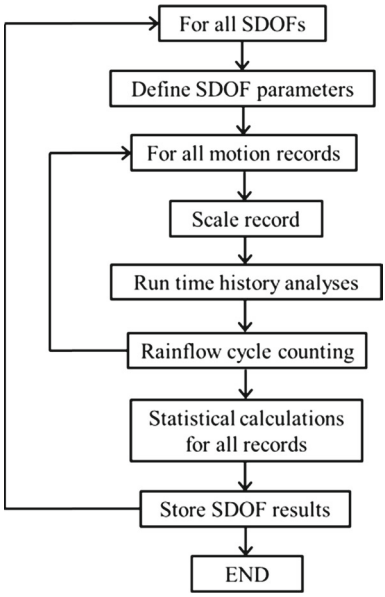

Fig. 2 Flowchart of Protocol.m

The elastic model is used for all structural systems expected to respond in the elastic domain even for the 2/50 seismic hazard level.

Table 2 summarises the range of periods of vibration T and post-yield stiffness ratios r (ratio of post-yield to elastic stiffness) of the SDOF systems that are considered in this study. The period range reflects typical fundamental periods of a large portion of the existing building stock in Europe. The lowest period for RC frames is taken equal to 0.15 s and not 0.10 s as for the other structural systems. This is in line with the empirical formula in EC8-Part 1 (§4.3.3.2.2(3)) for estimating the fundamental period of vibration for single storey RC frames. Moreover, higher post-yield stiffness ratios have been adopted for timber walls than for other structural systems in accordance with experimental results by Stewart (1987).

The q-factors (Table 2) have been chosen following the recommendations in EC8-Part 1. The yield strength F_y of the SDOF systems is calculated from the ordinate of the EC8 design spectrum for the 10/50 seismic hazard level, the period T and the q-factor of the SDOF system. The viscous damping ratio ζ is assumed equal to 5 % for all structural systems. In total, 567 different SDOF systems are examined.

4 Calculation of seismic demands

This section evaluates the cumulative seismic demands imposed on the structural systems by the scaled ground motion records. To serve this goal, an application named Protocol.m is developed in MATLAB v7.11 (2010), the flowchart of which is presented in Fig. 2. In the following, the steps of the algorithm that were not covered in previous sections are outlined.

4.1 Time history analyses

Linear and nonlinear time history analyses were carried out by means of the software RUAUMOKO (Carr 2012) using the Newmark constant acceleration integration algorithm

and an analysis time step of 0.001 s. Tangent stiffness proportional damping was applied as recommended by Priestley and Grant (2005). For each combination of SDOF system and ground motion record, Protocol.m writes the input file, executes RUAUMOKO and reads the output results. In total, 567 (SDOFs) × 80 (ground motions) = 45,360 time history analyses were conducted.

4.2 Rainflow cycle counting

Cumulative seismic damage effects are a function of the number, ranges, means and sequence of the imposed deformation cycles (Krawinkler et al. 2001). To determine the first three parameters, all displacement responses obtained by time history analyses of the SDOF systems are re-arranged using the simple rainflow cycle counting algorithm by Dowing and Socie (1982). This method identifies cycles as closed hysteretic loops and provides their ranges (difference between maximum and minimum peak) and means (average value of minimum and maximum peak).

The calculated cycle ranges are centred with respect to zero and normalized with respect to the maximum cycle range divided by two. This assumes that the cycle means are close to zero and the displacement history can be approximated by symmetric cycles around a zero mean. This assumption is made in many previous studies (e.g. Krawinkler et al. 2001; FEMA-461 2007) and it is supported by the time history analysis results obtained in this study. Finally, normalized cycle ranges are arranged in descending order.

The afore-described methodology does not account for the sequence of the imposed cycles, which may become important for inelastic systems because their performance depends on the history of the previously applied damaging cycles (Krawinkler 2009). In this study, sequence effects are considered in an approximate manner by assuming that only pre-peak excursions cause structural damage and post-peak cycles are therefore neglected (Krawinkler et al. 2001; FEMA-461 2007). Pre-peak excursions are excursions before the last of the maximum or minimum displacement peak response. Limiting the cycles considered for loading protocols to pre-peak excursions only is based on the observation that cumulative seismic damage is caused mainly by 'primary' excursions that widen the envelope of response in the positive or negative direction (Krawinkler et al. 2001). Post-peak cycles are therefore assumed to cause only minor additional damage. On the other hand, all pre-peak excursions are considered as 'primary' excursions that impose larger demands than previous cycles and therefore cause significant structural damage. Hence, neglecting the post-peak cycles but considering all pre-peak cycles as primary excursions under- and over-estimates the damaging effect of real cycle sequences respectively and therefore the two assumptions balance each other to some extent.

Figure 3 summarizes the adopted methodology for a timber wall SDOF system with fundamental period T = 0.20 s, post-yield stiffness ratio r = 1 % and q-factor = 1, which is subjected to the Umbria Marche (1997) aftershock ground motion record (M_w = 5.6, R = 13 km, PGA = 0.09 g, Soil type C). Figure 3a presents the first 20 s of the ground motion and Fig. 3b and c the lateral displacement and force responses of the SDOF system, respectively. In Fig. 3b the pre-peak response that will be used for determining the imposed cycle demands is highlighted. Figure 3d presents the force versus displacement hysteretic response. Following Wayne Stewart's hysteretic model, this response is characterized by significant pinching and cyclic strength deterioration. Note that inelastic response is developed despite the fact that this SDOF system was designed for q = 1. The SDOF system responds in the inelastic range because it is examined for the 2/50 seismic hazard level while it was designed for the 10/50 seismic hazard level.

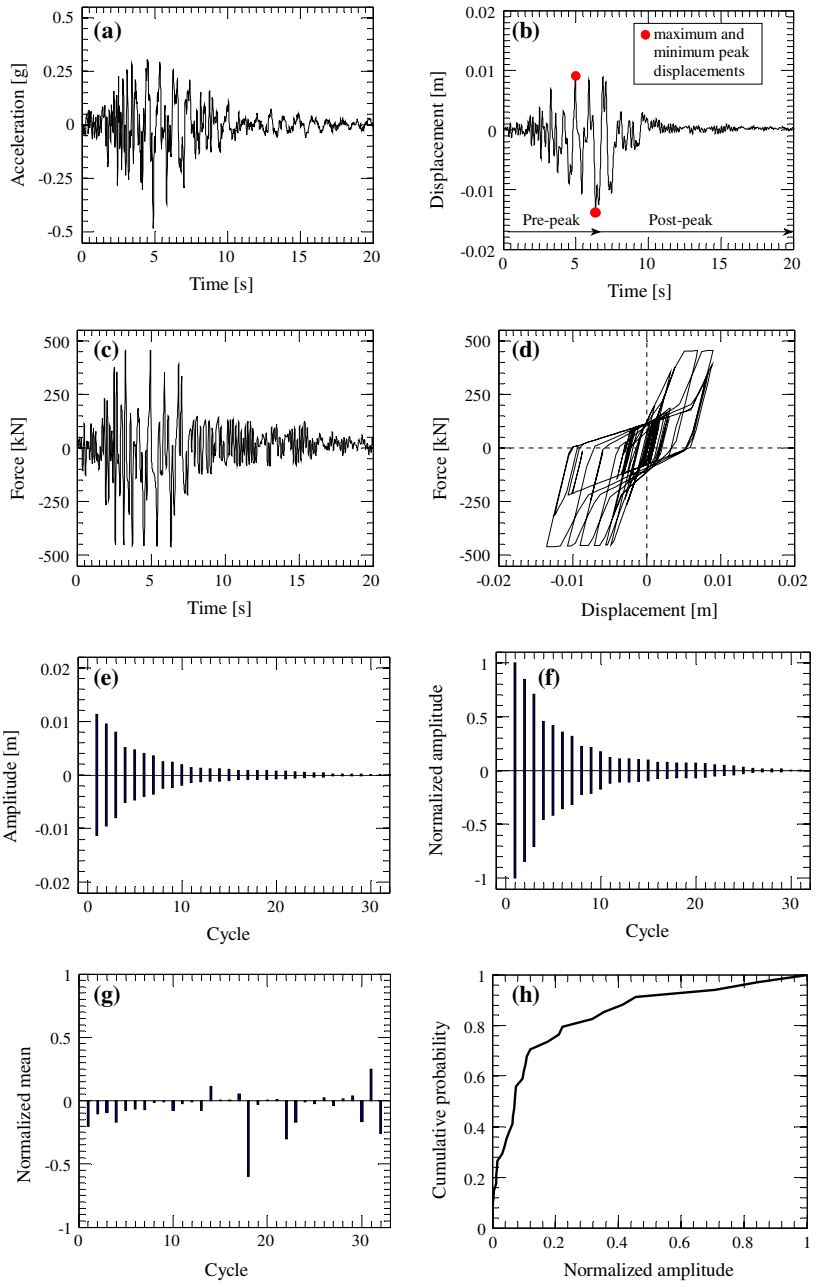

Fig. 3 Seismic demand on an example SDOF system representing a timber wall building with T = 0.20 s, r = 1 % and q = 1 subjected to the Umbria Marche (1997) aftershock record: **a** ground motion record; **b** lateral displacement response; **c** lateral force response; **d** force-displacement hysteretic response; **e** ordered cycle amplitudes; **f** ordered normalized cycle amplitudes; **g** normalized cycle means; **h** empirical cumulative distribution function (CDF) of cycle normalized amplitudes

Figure 3e presents displacement cycle amplitudes, which are defined in the following as cycle ranges divided by 2. Cycle ranges are determined by the rainflow cycle counting method for the pre-peak displacement response of Fig. 3b, then they are centred with respect to zero and finally they are placed in descending order. For example, using rainflow counting, the range of the maximum cycle of the pre-peak displacement response in Fig. 3b was calculated to be 0.022 m. This results in a symmetric cycle with a displacement amplitude of 0.011 m around a zero mean. In addition, Fig. 3f shows the same amplitudes normalized with respect to the maximum amplitude. As a result, normalized amplitudes of the first cycle are equal to 1 and of the remaining cycles <1.

Figure 3g presents calculated cycle means normalized with respect to the maximum cycle amplitude. Cycle numbers correspond to the ones of Fig. 3e, f. The figure shows that for the first cycles, which have important amplitudes, cycle means are close to zero which supports the adopted simplification of neglecting the effect of the mean value when deriving standardized loading histories. In the same figure, it can be seen that the mean of the 18th cycle is significant. However, the range of this cycle is very small as depicted in Fig. 3f and the effect of this cycle on the whole response therefore rather negligible.

Figure 3h illustrates the obtained CDF of the normalized amplitudes. It shows that 90 % of the cycles have amplitudes smaller than 50 % of the maximum cycle's amplitude. Hence, the majority of cycles have rather small amplitudes.

4.3 Statistical evaluation of normalized cycle amplitudes

As proposed by FEMA-461, the loading protocols will reflect the median values of the normalized cycle amplitudes. This is in good agreement with EC8-Part 1 (§4.3.3.4.3(4)) which allows that the average value of all analyses is used as design value if the response is obtained from more than seven different accelerograms.

To analyse the data of each SDOF system, the median values of the normalized cycle amplitudes of the two sets of records are evaluated. The first set comprises the 60 ground motion records for the low to moderate seismicity case (see Table 1) and the second set the 20 ground motion records for the high seismicity case (Krawinkler et al. 2001). The median normalized cycle amplitudes are calculated as the median of the 1st, 2nd, 3rd,... largest cycle of all ground motion records of one set (FEMA-461 2007). As all amplitudes have been normalized by the maximum amplitude and arranged in descending order, the amplitudes of all first cycles are equal to one and therefore also their median is equal to one. For the 2nd, 3rd, ... largest cycle the median values of the normalized amplitudes are always smaller than one.

Figure 4a presents the medians of normalized cycle amplitudes for the example SDOF system of the previous section and the low to moderate seismicity records. Only damaging cycles are shown. Damaging cycles are considered herein as cycles with amplitudes greater than a threshold value below which imposed damage may be considered negligible. Clearly, the latter limit depends on many parameters. Following the assumption by Krawinkler et al. (2001), cycles with normalized amplitudes $>\delta_o = 0.05$ are considered as damaging in this study.

Figure 4b presents a comparison of median normalized cycle amplitudes and median cycle means normalized again to the maximum cycle amplitude for the same SDOF system. From this figure it is evident that median normalized cycle means remain constantly close to zero (maximum value is 0.12). Hence, mean effects (i.e. asymmetric cycles) can be ignored with reasonable accuracy as mentioned before. This may be attributed first to the fact that only ordinary and not near fault records are examined and second to the fact that only pre-peak

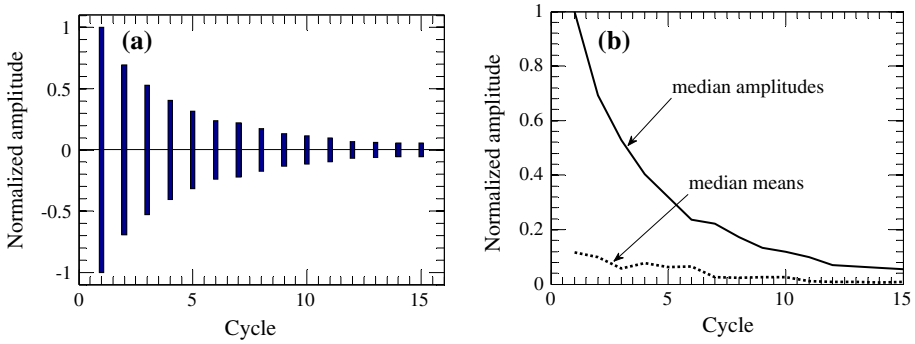

Fig. 4 Statistical measures of normalized cycle amplitudes for an SDOF system representing a timber wall building with T = 0.2 s, r = 1 %, q = 1 and the low to moderate ground motion records: **a** median normalized amplitudes ordered sequence; **b** comparison of normalized median cycle amplitudes and normalized median cycle means

response is examined in this study. Mean effects become more important as the degree of inelasticity (q-factor) increases. However, Sect. 5 will show that construction of loading protocols is governed by SDOF systems with low q-factors.

4.4 Parametric analyses of SDOF systems

After evaluating the statistical measures of normalized cycle amplitudes, parametric analyses are conducted in order to determine the most critical SDOF systems in terms of cumulative seismic demands. Two important cumulative demand parameters are examined herein, namely the number of damaging cycles N and the sum of normalized cycle amplitudes $\Sigma\delta_i$ as determined by the median normalized cycle amplitude sequences of the SDOF systems evaluated in the previous section (see Fig. 4a). The same parameters for determining cumulative damage demands have been used in several previous loading protocol studies (e.g. Richards and Uang 2006).

Figures 5 and 6 present $\Sigma\delta_i$ and N of several SDOF systems for the low to moderate seismicity ground motion set. The cumulative demand parameters $\Sigma\delta_i$ and N follow in general similar trends. The plots show, for example, that both parameters decrease rapidly with period in the short period range (<0.5 s) and flatten out for longer periods (Figs. 5a, 6a). Similar trends can be observed for the variation of the cumulative demand parameters with increasing q-factor (Figs. 5b, 6b). In these figures, the values for $q \rightarrow 0$ represent the response of elastic SDOF systems with infinite strength. It can be seen that elastic systems are subjected to the largest cumulative seismic demands followed by systems with q-factors equal to unity. For q-factors between 1 and 3, cumulative demands drop rapidly, while for high q-factors (>3) they tend to stabilize.

Figures 5c and 6c show that the cumulative seismic demand parameters tend to increase slightly as the post-yield stiffness ratio increases. This is in line with the observation that the elastic system is subjected to the largest cumulative demands, since the elastic system can be considered as a limit case with a post-yield stiffness ratio equal to unity.

Finally, Figs. 5d and 6d compare $\Sigma\delta_i$ and N values for the different hysteretic models that are included in this study in order to represent different structural systems (see Sect. 3). It can be seen that the elastic system develops the highest cumulative demands followed by the Wayne Stewart, the 'thin' Takeda and the 'fat' Takeda hysteretic models. The flag-shaped hysteretic model develops the smallest cumulative seismic demands.

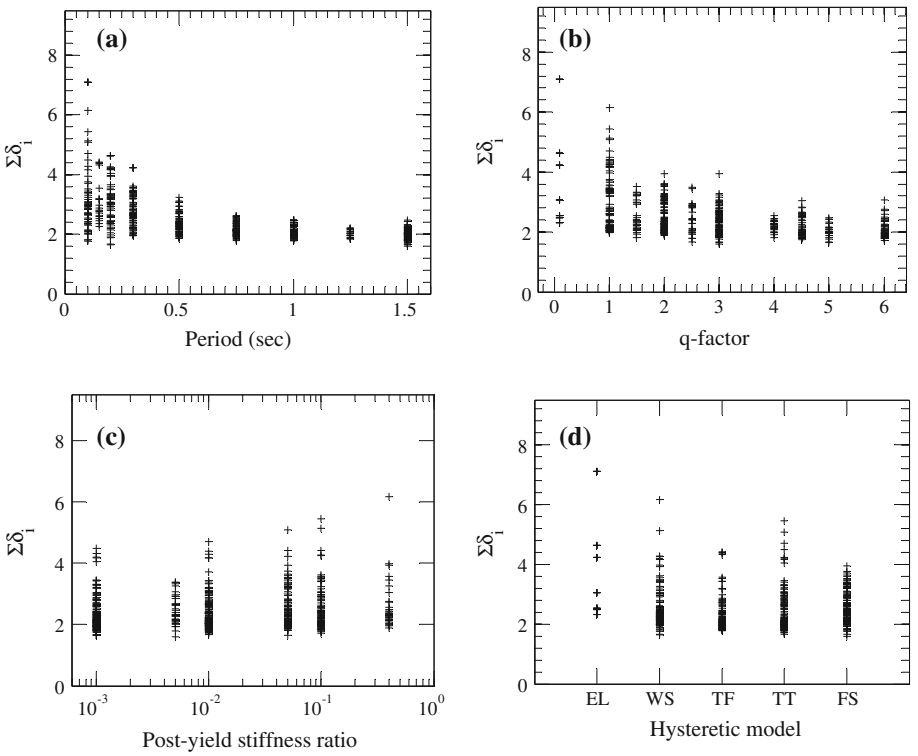

Fig. 5 Variation of the sum of normalized displacements $\Sigma\,\delta_i$ of the median normalized amplitude sequences for the low to moderate seismicity earthquakes with: **a** vibration periods; **b** q-factors; **c** hardening ratios and **d** hysteretic models of the SDOF systems

Figure 7 compares the cumulative demand parameters of the median normalized cycle amplitude sequences as derived from the 60 low to moderate seismicity ground motion records (see Table 1) with those from the 20 high seismicity records (Krawinkler et al. 2001). The figure clearly underscores that high seismicity records impose higher cumulative demands than low to moderate seismicity records. This applies in particular to the elastic systems or systems responding in the low ductility range, which are also the systems subjected to the largest cumulative demands and which will therefore govern the design of loading protocols. This finding advocates the usage of different loading protocols for low to moderate seismicity regions and high seismicity regions. It is recalled that Fig. 7a refers to the sum of normalized cycle amplitudes with respect to Δ_{max}. A comparison of the sum of non-normalized cycle amplitudes $\Sigma\,\Delta_i$ would of course be much more severe for the high seismicity records.

5 Construction of loading protocols

This section describes the development of the new loading protocols. First, the methodology for constructing loading protocols to meet cumulative seismic demands of a specific SDOF system is outlined (Sect. 5.1). Next, the proposed loading protocols corresponding to the critical SDOF systems are presented (see Sect. 5.2).

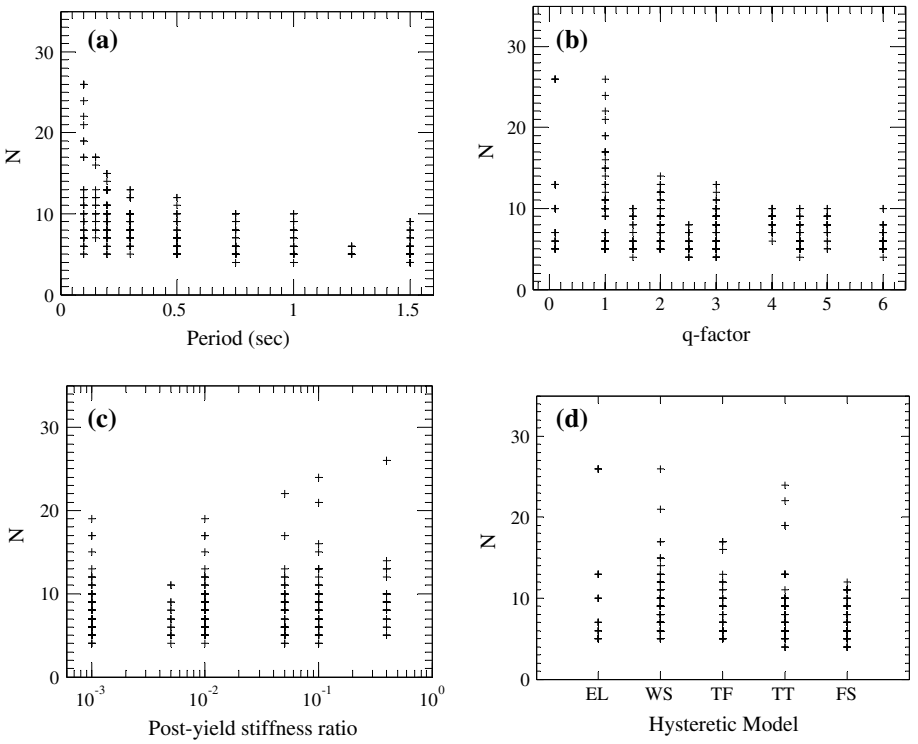

Fig. 6 Variation of the number of damaging cycles of the median normalized amplitude sequences for the low to moderate seismicity earthquakes with: **a** vibration periods; **b** q-factors; **c** hardening ratios and **d** hysteretic models of the SDOF systems

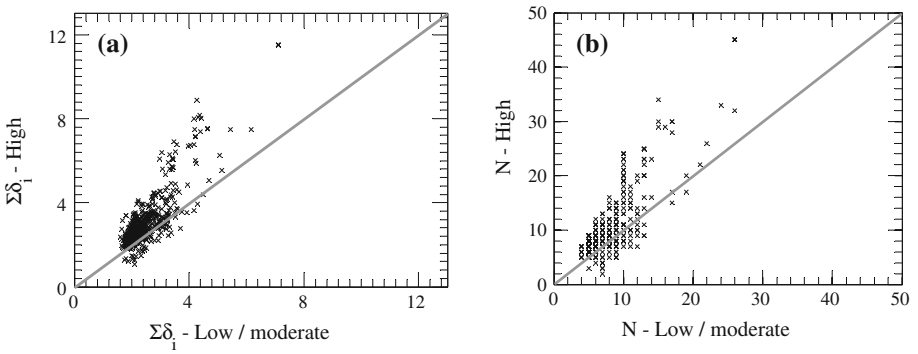

Fig. 7 Comparison of cumulative seismic demand parameters calculated for low to moderate and high seismicity regions: **a** $\Sigma\delta_i$; **b** N. Each point represents the cumulative damage parameters of a particular SDOF system calculated from its median normalized cycle amplitude sequence

5.1 Methodology for constructing loading protocols

The algorithm for constructing loading protocols (Fig. 8) developed in this study aims at describing the normalized ordered amplitude sequence of the SDOF system (Fig. 4a) as an

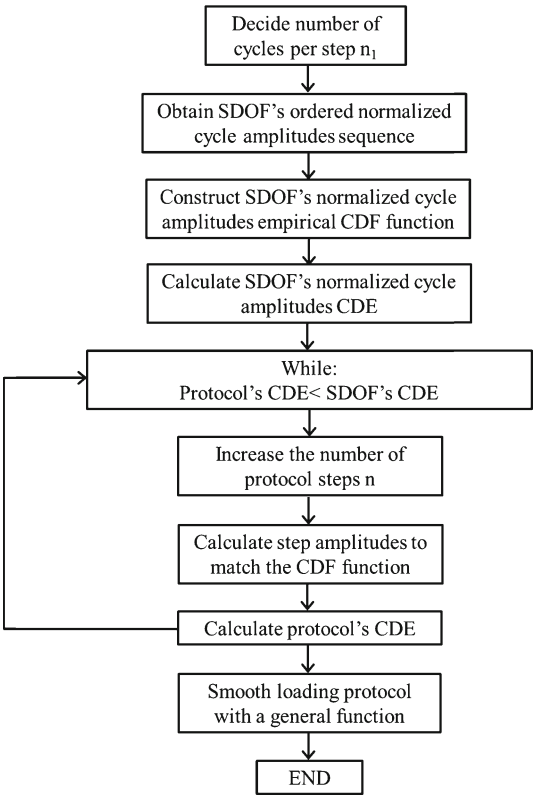

Fig. 8 Loading protocol construction methodology

analytical function with empirical coefficients. The loading protocol should yield a conservative distribution of normalized cycle amplitudes which tends to overestimate the CDE obtained from time history analysis. The method is based on similar procedures developed in previous studies on loading protocols (Richards and Uang 2006; Hutchinson et al. 2011). Unlike in previous studies, however, the amplitudes of the cycles of the loading protocol are expressed as analytical functions of the load step, which allows describing different loading protocols for different structural systems by only two parameters.

Each loading protocol consists of n load steps with n_1 cycles of the same amplitude per step. The loading protocol comprises therefore in total $n_{tot} = n \cdot n_1$ cycles. Before constructing the loading protocol, the number of cycles per step n_1 is chosen. Typically, two (e.g. FEMA-461) or three (e.g. ISO-21581) cycles per load step are assigned, which allows investigating the stiffness and strength degradation of the structural component that is tested. As the number of equal cycles per step decreases, the SDOF's ordered amplitude sequence obtained from time history analysis can be represented with higher accuracy. As a limit case, when each cycle is assigned a different amplitude, the actual SDOF's amplitude sequence can be obtained. In order to give the applicant the largest possible choice with regard to the form of the loading protocol, loading protocols for all three options (one, two and three cycles per step) will be developed.

The SDOF system's normalized amplitude sequence is obtained using the methodology described in Sect. 4.3 and the corresponding empirical CDF is constructed. The latter reflects the distribution of the median values of the normalized cycle amplitudes (Fig. 4b). Addition-

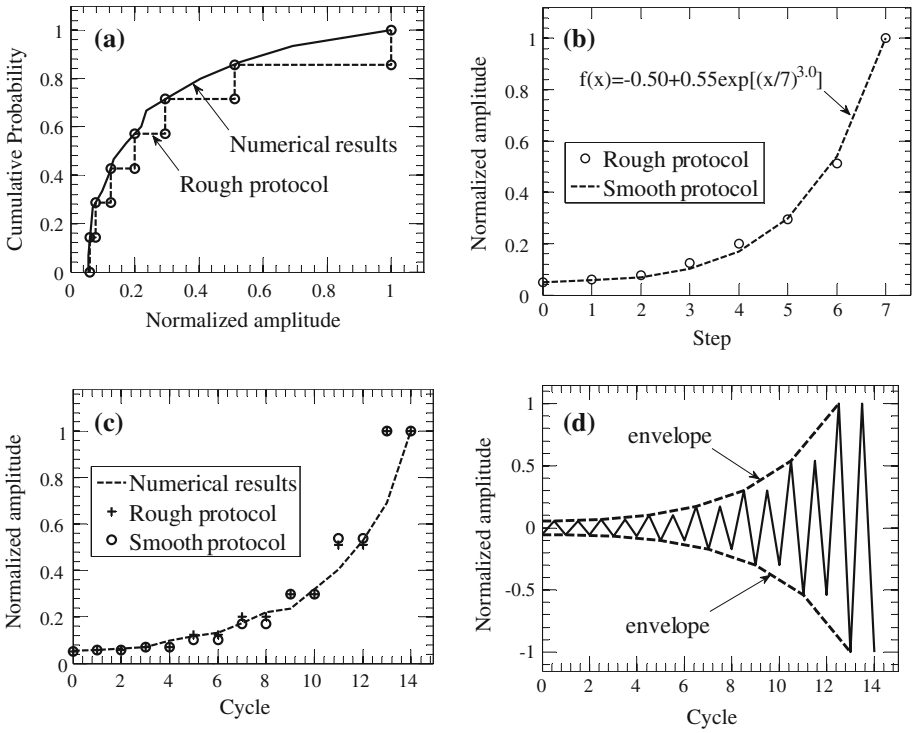

Fig. 9 Loading protocol construction: **a** comparison of loading protocol and numerical results normalized cycle amplitude CDFs; **b** comparison of rough and smooth protocol normalized load step amplitudes; **c** normalized cycle amplitude sequences of the numerical results, the rough and the smooth protocol and **d** derived normalized loading protocol

ally, the CDE of the SDOF system cycle sequence is calculated. The basis for calculating the CDE is the following general damage model, which is based on Miner's rule (Krawinkler et al. 2000; Richards and Uang 2006):

$$CDE = C \cdot \sum_{i=1}^{N} (\Delta_i)^c = C \cdot (\Delta_{\max})^c \cdot \sum_{i=1}^{N} (\delta_i)^c \tag{2}$$

where C and c are structural performance parameters. The parameter c is typically >1 reflecting the fact that larger cycles cause more structural damage than small cycles (Richards and Uang 2006).

As a first step when constructing the loading protocol, a while-loop is launched, where the number of total steps n progressively increases. For each value of n, first the protocol cycle step amplitudes are determined to match SDOF's and protocol's CDF for each load step (see Fig. 9a) and then protocol's CDE is calculated. The while-loop terminates when protocol's CDE exceeds for the first time SDOF's CDE.

For the construction of loading protocols, the value of c is assumed as 1. If a protocol's CDE exceeds the SDOF's CDE for $c = 1$, then the same holds for all values of $c > 1$. This applies because the proposed methodology for deriving the loading protocol tends to impose more cycles with large amplitudes than resulted from the numerical analyses of the SDOF

systems (Fig. 9a). Hence, c = 1 may be considered a conservative assumption. As only the relative and not the absolute magnitude of the CDE is of interest, the choice of C is irrelevant.

Figure 9 presents the loading protocol development for the median normalized amplitude sequence of the SDOF system described in Sect. 4.3 (Fig. 4a). For two cycles per step, the algorithm yields 7 steps (14 cycles in total). Figure 9a presents for this SDOF system the comparison of the CDF as obtained from the numerical results and as calculated from the derived protocol. The loading protocol CDF meets the SDOF's CDF at the end of each load step (every two cycles). In this manner, the loading protocol's CDF approaches and remains always below the SDOF's CDF. This is on the conservative side since it indicates that the protocol comprises always a higher percentage of large amplitude cycles, which are more damaging than small amplitude cycles.

The previous methodology yields arbitrary loading protocol cycle amplitudes which may change abruptly between two subsequent load steps ('rough' loading protocol). In order to smooth the loading protocol curve, the following general exponential function is fitted to the rough protocols:

$$f(t) = \frac{1}{e-1} \cdot \left[\delta_o \cdot e - 1 + (1 - \delta_o) \cdot \exp\left(t^{\alpha}\right)\right] \tag{3}$$

where δ_o is the threshold for damaging cycles (assumed 0.05 herein), t = x/n, x is the current load step, n is the number of load steps and α is a parameter describing the rate of amplitude increase. The proposed function approaches for t = 0 the threshold value δ_o and for t = 1 unity. Hence, it always satisfies the boundary conditions of the loading protocols proposed in this study. The form of Eq. (3) was chosen because it yields in almost all cases superior fits than polynomial or power functions. Substituting $\delta_o = 0.05$ and t = x/n into Eq. (3), one obtains:

$$f(x) = -0.50 + 0.55 \cdot \exp\left[\left(\frac{x}{n}\right)^{\alpha}\right] \tag{4}$$

Equation (4) requires only two parameters (i.e. n and α) for fully determining the normalized loading protocol sequence. The number of load steps n is determined from the algorithm shown in Fig. 8. The parameter α is calculated in order to provide the best fit between the 'rough' and the 'smooth' protocol, which minimizes the sum of squared errors between the predictions of Eq. (4) and the normalized amplitudes of the 'rough' protocol.

Figure 9b compares for the example SDOF system the predictions of Eq. (4) for n = 7 and α = 3.00 with the normalized amplitudes of the rough protocol and shows that the amplitudes of the rough and smooth protocol do not differ significantly. Furthermore, Fig. 9c compares the normalized cycle amplitudes of the SDOF system as derived from the numerical analyses (placed now in ascending order for comparison purposes), with the normalized cycle amplitudes of the rough and the smooth protocol. The protocols follow closely the SDOF's median response, yet remaining conservative for the large cycle amplitudes.

Finally, Fig. 9d illustrates the derived smooth normalized loading protocol. It consists of 7 load steps of 2 equal cycles yielding 14 cycles in total. The amplitudes are determined by the envelope function defined by Eq. (4) for n = 7 and α = 3.00. Note that x in Eq. (4) is the load step and not the cycle.

5.2 New loading protocols

This section presents new loading protocols for quasi-static cyclic testing which were developed following the methodology outlined in the previous section. Most existing loading protocols were developed in order to meet the demands on the structural system that is subjected to the largest cumulative damage demand. However, this results inevitably in overly

demanding protocols for all other structural systems. Existing protocols feature further a fixed number of cycles per load steps. The new loading protocols limit these drawbacks by developing the loading protocols as functions of seismicity (low to moderate vs. high), period and hysteretic model. For each of these combinations, the loading protocol is developed for the pair of q-factor and post-yield stiffness ratio that yields the largest CDE. In addition, the new loading protocols allow to choose between one, two and three cycles per step.

Table 3 summarizes the resulting protocol parameters n and α that were derived from the median values of cumulative damage demands for different structural configurations, levels of seismicity and cycles per load step. It is recalled that α describes the increase in amplitude with load step and n the number of load steps. If, for example, two cycles per load step are assigned, the total number of cycles n_{tot} is 2n. For short natural periods, cumulative damage demands decrease with period (Figs. 5a, 6a). For periods longer than $T = 0.5\,s$, however, cumulative damage demands tend to converge towards a constant value. Hence, for systems with $T \geq 0.5\,s$, protocols derived for $T = 0.5\,s$ will be adopted. The slight conservatism resulting for longer period structures may compensate partly for the higher mode effects of long-period MDOF systems as explained in Sect. 3. It is however recalled that the proposed loading protocols cannot represent structural systems with significant higher mode effects or MDOF systems with a significant concentration of inelastic deformations (e.g. structures forming soft storey mechanisms).

The loading protocols proposed in Table 3 are all normalized with respect to the maximum displacement Δ_{max}. Before performing a quasi-static cyclic test, Δ_{max} needs to be estimated. Since the cumulative demand was determined for the seismic hazard corresponding to the NC limit state, the parameter Δ_{max} corresponds to the displacement capacity of the specimen which EC8-Part 3 (2005) defines as the displacement associated with a strength loss of 20 % of its maximum strength. This displacement can be estimated by analytical, numerical or empirical models or by performing first a monotonic test and then assigning an appropriate reduction factor, which relates cyclic to monotonic displacement capacities. If Δ_{max} is attained during the experiment without significant loss of strength it is suggested to continue the loading scheme until the strength loss exceeds 20 % of the maximum strength.

Clearly, a good estimation of Δ_{max} prior to testing is important for the construction of the loading protocols. This is not a limitation of the adopted methodology for deriving loading protocols, but a general issue of all cyclic loading protocols arising from the fact that structural capacities depend on cumulative damage demands (Krawinkler 2009). Ideally, an iterative procedure is required, where several loading protocols are applied to the same type of specimen and the assumed Δ_{max} is constantly updated until it matches the experimental displacement capacity with adequate accuracy. However, as shown in Krawinkler et al. (2001), the normalized cumulative damage demands are not very sensitive to Δ_{max}. Hence, as long as the number of load steps to failure is closely predicted, the proposed loading protocols are expected to yield realistic estimates of the examined structural capacities.

As an alternative Δ_{max} can be taken as the target displacement demand for which the structural component is to be qualified (Krawinkler 2009). This displacement may be determined by nonlinear time history analyses or simpler methods like the capacity spectrum method (Freeman 2004) or the displacement coefficient method (FEMA-273 1997). In this case, the loading protocols can be used to verify the adequacy of the test specimen for the specific seismic demand.

As example, loading protocols for a structure with RC shear walls and $T = 0.2\,s$ are constructed. Table 3 shows the corresponding loading protocol parameters for one to three cycles per load step: $n = 13$ and $\alpha = 2.3$ when $n_1 = 1$, $n = 6$ and $\alpha = 2.26$ when $n_1 = 2$ and $n = 3$ and $\alpha = 2.2$ when $n_1 = 3$. Using the approach in EC8-Part 3, the NC chord rotation

Table 3 Proposed loading protocol parameters for different structural systems and levels of seismicity

Structural system-Hysteretic model	Vibration period (sec)	Low to moderate seismicity			High seismicity		
		n_1=1	n_1=2	n_1=3	n_1=1	n_1=2	n_1=3
Infinitely elastic-Elastic (EL)	T=0.1s	n=26 α=3.05	n=12 α=3.05	n=8 α=3.01	n=45 α=3.24	n=22 α=3.22	n=14 α=3.25
	T=0.2s	n=14 α=1.96	n=6 α=2.00	n=4 α=1.87	n=25 α=2.42	n=12 α=2.44	n=8 α=2.36
	T=0.3s	n=10 α=1.49	n=5 α=1.45	n=3 α=1.45	n=24 α=2.51	n=12 α=2.49	n=7 α=2.52
	T≥0.5s	n=7 α=1.58	n=3 α=1.56	n=2 α=1.60	n=11 α=2.01	n=5 α=1.98	n=3 α=2.03
Timber walls-Wayne Stewart (WS)	T=0.1s	n=27 α=3.94	n=12 α=3.97	n=7 α=3.81	n=32 α=3.62	n=15 α=3.58	n=9 α=3.49
	T=0.2s	n=15 α=2.96	n=7 α=2.93	n=4 α=2.85	n=34 α=3.22	n=16 α=3.21	n=10 α=3.21
	T=0.3s	n=13 α=3.16	n=6 α=2.98	n=3 α=2.71	n=23 α=2.44	n=11 α=2.4	n=7 α=2.45
	T≥0.5s	n=11 α=3.16	n=5 α=3.07	n=2 α=2.48	n=14 α=2.91	n=6 α=2.75	n=3 α=2.56
RC frames-Fat Takeda (FT)	T=0.15s	n=16 α=3.37	n=7 α=3.3	n=4 α=2.93	n=30 α=2.82	n=14 α=2.80	n=9 α=2.78
	T=0.3s	n=10 α=1.98	n=5 α=1.96	n=2 α=1.85	n=20 α=2.0	n=10 α=1.94	n=6 α=1.9
	T≥0.5s	n=6 α=2.06	n=2 α=1.66	n=2 α=1.66	n=12 α=2.57	n=5 α=2.40	n=3 α=2.43
RC & masonry shear walls-Thin Takeda (TT)	T=0.1s	n=24 α=4.23	n=11 α=4.17	n=6 α=4.03	n=33 α=4.24	n=16 α=4.19	n=10 α=4.11
	T=0.2s	n=13 α=2.3	n=6 α=2.26	n=3 α=2.2	n=23 α=2.63	n=11 α=2.66	n=7 α=2.55
	T=0.3s	n=10 α=2.15	n=5 α=2.16	n=2 α=2.22	n=20 α=2.3	n=10 α=2.28	n=6 α=2.3
	T≥0.5s	n=7 α=1.7	n=3 α=1.63	n=2 α=1.69	n=13 α=2.23	n=6 α=2.27	n=3 α=2.06
Masonry rocking walls-Flag-shaped (FS)	T=0.1s	n=8 α=1.2	n=4 α=1.21	n=2 α=1.21	n=15 α=2.3	n=7 α=2.25	n=4 α=2.38
	T=0.2s	n=12 α=2.28	n=5 α=2.25	n=3 α=2.36	n=16 α=3.05	n=7 α=2.96	n=4 α=2.92
	T=0.3s	n=9 α=1.89	n=4 α=1.83	n=2 α=1.85	n=17 α=2.85	n=8 α=2.86	n=5 α=2.83
	T≥0.5s	n=6 α=1.51	n=3 α=1.63	n=2 α=1.31	n=10 α=2.02	n=5 α=2.03	n=2 α=1.73

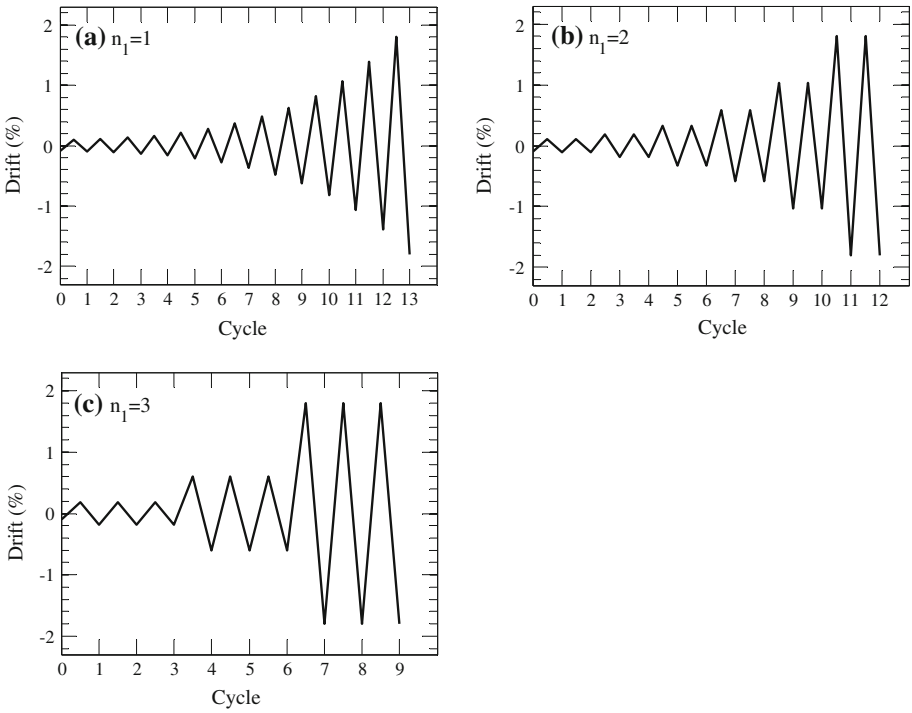

Fig. 10 Example loading protocols for an URM structure with elastic period of vibration T = 0.2 s in a region of low to moderate seismicity **a** one cycle per step; **b** two cycles per step; **c** three cycles per step

capacity of the RC shear wall is estimated as 1.8 %. The resulting loading protocols for this SDOF system are presented in Fig. 10a–c.

The amplitudes of the load steps are:

- One cycle per load step ($n_1 = 1$): 0.10, 0.11, 0.13, 0.17, 0.21, 0.28, 0.37, 0.48, 0.63, 0.82, 1.07, 1.38, 1.80 %
- Two cycles per load step ($n_1 = 2$): 0.12, 0.18, 0.33, 0.59, 1.03, 1.80 %
- Three cycles per load step ($n_1 = 3$): 0.19, 0.60, 1.80 %

Since the new loading protocols account for the effect of the fundamental period on cumulative demand, some judgment is required when planning a test series with several test specimens: In order to facilitate the comparison of experimental results within one test series, it might be desirable to subject all test specimens to the same loading protocol although they might represent elements in structural systems with different fundamental periods. This could, for example, be the case if a series of RC walls of different dimensions or different axial load ratios are tested, which are derived from reference buildings of different heights and therefore most likely also different fundamental periods. Although this paper does not define a single protocol for such a case, the parameters in Table 3 will permit investigating the range of loading protocols that are advisable and hence offer some guidance for designing the loading protocol for the test series. A common choice might of course be the loading protocol that leads to the largest cumulative damage demand.

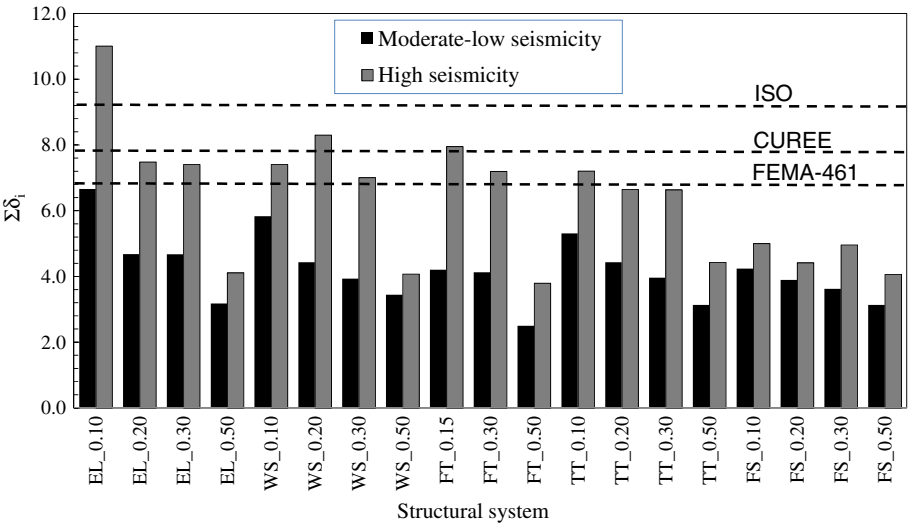

Fig. 11 Comparison of proposed and existing loading protocols in terms of $\Sigma\delta_i$

6 Comparisons of the proposed loading protocols with existing loading protocols

This section identifies trends in the proposed loading protocols and compare them to three well established loading protocols for quasi-static cyclic testing: the CUREE protocol developed for woodframed shear wall structures and ordinary ground motions (Krawinkler et al. 2001); the FEMA-461 displacement controlled protocol for drift sensitive non-structural components (FEMA-461 2007); and the ISO-21581 (ISO 2010) protocol for timber shear wall structures. All these protocols express the loading history as a function of the peak displacement which facilitates the comparison.

Figure 11 compares the new and existing protocols in terms of the sums of normalized displacements $\Sigma\delta_i$. This cumulative damage parameter is chosen because it contains information on the number and amplitudes of the cycles in the loading protocol. In this figure, structural systems are annotated with two letters followed by a decimal number. The two letters identify the hysteretic model (see Table 2) and the decimal number represent the natural period in seconds. Note that—unlike the new protocols—the CUREE, FEMA-261 and the ISO-21581 protocols are all independent of the structure's fundamental period. The new protocols are all evaluated for two cycles per load step.

The figure shows that the new protocols for low to moderate seismicity impose always significantly lower cumulative damage demands than the new protocols for high seismicity. Figure 11 shows further that $\Sigma\delta_i$ tends to decrease as the period of vibration increases. As a result, the $\Sigma\delta_i$ demands for periods equal to or longer than 0.5 s are significantly smaller than the $\Sigma\delta_i$ demands for periods between 0.1 and 0.3 s.

When the new protocols are compared to the existing ones (CUREE, FEMA-461 and ISO-21581), one notices that the new protocols for regions of low to moderate seismicity are, as expected, significantly less demanding than the existing loading protocols. Hence, the application of the new protocols for low to moderate seismicity may lead to less conservative estimations of structural capacities. The CUREE and FEMA-461 loading protocols impose similar cumulative demands than the new protocols for high seismicity if the period of vibration is <0.5 s. CUREE and FEMA-461 are less demanding for stiff elastic systems

(T = 0.1 s) in high seismicity regions and more demanding for all flag-shaped hysteretic systems. Note, however, that the CUREE protocol includes primary and secondary cycles and therefore the parameter $\Sigma\delta_i$ overestimates its actual CDE since secondary cycles generate less damage than primary cycles. The ISO-21581 protocol imposes a significantly larger CDE than the new protocols on all structural systems apart from the stiff elastic system with T = 0.1 s in high seismicity regions.

7 Conclusions

Seismic strength and deformation capacities of structural members are often quantified by means of quasi-static cyclic tests. In these tests, predefined displacement histories, named loading protocols, are imposed at slow rates. Since strength and in particular deformation capacity of structural members are dependent on the cumulative damage demand, loading protocols should impose cumulative damage demands similar to the ones imposed by real earthquakes.

In this study, two different ground motion sets are employed. The first set consists of 60 records (see Table 1) and is representative of low to moderate seismicity regions in Europe for the hazard level 2/50. The second ground motion set is a set that was used in previous studies on loading protocols for high seismicity regions (Krawinkler et al. 2001). In a parametric study, the ground motions are applied to a large variety of SDOF systems representing the majority of buildings in European regions. The results reveal the strong dependence of the cumulative seismic demand on the level of seismicity (low to moderate vs. high) as well as on several structural parameters of the SDOF systems such as the period of vibration, the behaviour factor (as a measure of the inelasticity the system is subjected to), the post-yield stiffness ratio and the type of the hysteretic response.

Using a new algorithm, loading protocols are developed as a function of the seismicity, the hysteretic model, the fundamental period and the number of cycles per load step (one, two or three). All loading protocols follow the same analytical form which requires only two parameters to define the amplitudes of each load step. Adopting this approach instead of proposing a single protocol provides more representative and less conservative loading protocols for the different structural systems and levels of seismicity. The new protocols allow, in addition, to choose between one to three cycles per load step.

Comparisons of the proposed loading protocols for regions of low to moderate seismicity with protocols well established in experimental testing (CUREE 2001; FEMA-461 2007; ISO 2010) show that the latter impose significantly higher cumulative damage demands. This may lead to an underestimation of the test specimen's strength and especially deformation capacity for regions of low to moderate seismicity. For regions of high seismicity, existing (CUREE 2001; FEMA-461 2007) and proposed loading protocols impose similar cumulative demands for the majority of structural systems. This is expected since existing protocols were derived for high seismicity regions. However, since existing protocols are not dependent on the fundamental period of the structure, they yield for long period structures a larger cumulative damage demand than the new loading protocols for high seismicity regions.

Acknowledgments The authors thank the two reviewers for their comments that helped to improve the manuscript. Financial support for this research was provided by the Swiss National Science Foundation within project NRP-66 (Resource Wood, Project No. 406640-136900). The opinions, findings, and conclusions expressed in this paper are those of the authors and do not necessarily reflect those of the sponsoring organization.

References

Aldemir A, Eberik MA, Demirel O, Sucuoğlu H (2013) Seismic performance assessment of unreinforced masonry buildings with a hybrid modeling approach. Earthq Spectra 29(1):33–57

Ali Q, Khan AN, Ashraf M, Ahmed A, Alam B, Ahmad N, Javed M, Rahman S, Fahim M, Umar M (2014) Seismic performance of stone masonry buildings used in the Himalayan belt. Earthq Spectra (Preprint)

AISC (2005) Seismic provisions for structural steel buildings. American Institute for Steel Construction, Chicago

ATC-24 (1992) Guidelines for cyclic seismic testing of components of steel structures for buildings. Applied Technology Council, California

Ambraseys NN, Douglas J, Rinaldis D et al (2004) Dissemination of european strong motion data, vol 2. Engineering and Physical Sciences Research Council, UK

Behr RA, Belarbi A (1996) Seismic test methods for architectural glazing systems. Earthq Spectra 12(1):129–143

Carr AJ (2012) Ruaumoko—a computer program for inelastic time history analysis. Department of Civil Engineering, University of Canterbury, New Zealand

CEN (2004) Eurocode 8: design of structures for earthquake resistance, part 1: general rules, seismic actions and rules for buildings. European Standard EN 1998-1, Brussels

CEN (2005) Eurocode 8: design of structures for earthquake resistance, part 3: assessment and retrofitting of buildings. European Standard EN 1998-3, Brussels

Clark P, Frank K, Krawinkler H, Shaw R (1997) Protocol for fabrication, inspection, testing and documentation of beam-column connection tests and other experimental specimens. Report No. SAC/BD-97/02, Steel Project Background Document

Dowing SD, Socie DF (1982) Simple rainflow cycle counting algorithms. Int J Fatique 4(1):31–40

EN-12512 (2001) Timber structures-test methods. Cyclic testing of joints made with mechanical fasteners, European Committee for Standardization, Brussels

Fardis M (2009) Seismic design, assessment and retrofitting of concrete buildings. Springer, Dordrecht

Filiatrault A, Isoda H, Folz B (2003) Hysteretic damping of wood framed buildings. Eng Struct 25:461–471

FEMA-273 (1997) NEHRP guidelines for the seismic rehabilitation of buildings. Federal Emergency Management Agency, Washington

FEMA-461 (2007) Interim protocols for determining seismic performance characteristics of structural and nonstructural components through laboratory testing. Federal Emergency Management Agency, Washington

Freeman SA (2004) Review of the development of the capacity spectrum method. ISET J Earthq Technol 41:1–13

Frumento S, Magenes G, Morandi P, Calvi GM (2009) Interpretation of experimental shear tests on clay brick masonry walls and evaluation of q-factors for seismic design. Research Report No 02.09, IUSS Press, Pavia

Gatto K, Uang C (2003) Effects of loading protocol on the cyclic response of woodframe shearwalls. J Struct Eng 129(10):1384–1393

Giardini D, Wiemer S, Fäh D, Deichmann N (2004) Seismic hazard assessment of Switzerland. Swiss Seismological Service, Zurich

Hutchinson T, Zhang J, Charles E (2011) Development of a drift protocol for seismic performance evaluation considering a damage index concept. Earthq Spectra 27(4):1049–1076

Iervolino I, Maddaloni G, Cosenza E (2008) Eurocode 8 compliant real record sets for seismic analysis of structures. J Earthq Eng 12(1):54–90

ISO-21581 (2010) Timber structures-static and cyclic lateral load test methods for shear walls. International Standards Organization, Geneva

Kramer SL (1996) Geotechnical earthquake engineering. Prentice Hall, New Jersey

Krawinkler H, Gupta A, Medina R, Luco N (2000) Loading histories for seismic performance testing of SMRF components and assemblies. Report SAC/BD-00/10, SAC Joint Venture, California

Krawinkler H, Parisi F, Ibarra L, Ayoub A, Medina R (2001) Development of a testing protocol for woodframe structures. CUREE, publication No. W-02

Krawinkler H (2009) Loading histories for cyclic tests in support of performance assessment of structural components. In: 3rd International conference on advances in experimental structural engineering

MATLAB 7.1 (2010) The MathWorks Inc., Natick, MA

Priestley MJN, Calvi GM, Kowalsky MJ (2007) Direct displacement based seismic design of structures. IUSS Press, Pavia

Priestley MJN, Grant DN (2005) Viscous damping in seismic design and analysis. J Earthq Eng 9(suppl2):229–255

Porter ML (1987) Sequential phased displacement (SPD) procedure for TCCMAR testing. In: 3rd meeting of the joint technical coordinating committee on masonry research, US-Japan coordinated program

Retamales R, Mosqueda G, Filiatrault A, Reinhorn A (2011) Testing protocol for experimental seismic qualification of distributed non-structural systems. Earthq Spectra 27(3):835–856

Richards PW, Uang C (2006) Testing protocol for short links in eccentrically braced frames. J Struct Eng 132(8):1183–1191

SIA 261 (2003) Actions on structures. Swiss Society of Engineers and Architects, Zurich

Stewart WG (1987) The seismic design of plywood sheathed shear walls. Ph.D. Thesis, University of Canterbury, New Zealand